IRAQI Academic Scientific Journals
Samarra Journal of Pure and Applied Science
SJPAS
www.sjpas.com
p ISSN: 2663-7405
e ISSN: 2789-6838

Synthesis, Characterization, Antioxidant, DFT Calculations, and Molecular Docking of a Schiff Base and Its Metal (II) Nanocomplexes

Mohammad Hassan Abed[1], Lekaa K. Abdul Karem[2] and Maha Salih Hussein[3]
1 Department of Applied Chemistry, College of Applied Science, University of Samarra, Iraq
2 Department of Chemistry, College of Education for Pure Science, University of Baghdad, Iraq
3 Department of Chemistry, College of Education for Pure Science, University of Samarra, Iraq

https://doi.org/10.54153/sjpas.2026.v8i1.1196

Article Information

Received: 08/04/2025
Revised: 08/05/2025
Accepted: 15/5/2025
Published: 10/04/2026

Keywords:

DFT, Nano-complexes, Molecular Docking, Schiff bases, and HOMO-LUMO.

Corresponding Author

E-mail:

Mobile:
mohammed.h@uosamarra.edu.iq

Abstract

Schiff base ((E)-1,2-diphenyl-2-(pyridin-2-ylimino) nethan-1-ol) was synthesized from benzoin and 2-Aminopyridine, along with its Co (II), Ni (II), Cu (II), and Zn (II) complexes. synthesized compounds were characterized by ^{1}H-NMR, ^{13}C-NMR, FT-IR, Uv-Vis, and molar conductivity measurements. Additionally, Cu (II) and Ni (II) nanocomplexes were prepared using Pulsed Laser Ablation in Liquid (PLAL) and characterized via FESEM, EDX, and XRD. Their antioxidant activities were evaluated using IC_{50} values, compared against standard antioxidants and their bulk counterparts, while molecular docking studies explored binding interactions with VEGFR2—a key target in liver and kidney cancer treatments due to its role in angiogenesis. Furthermore, Density Functional Theory (DFT) calculations were carried out at the B3LYP level using the 6-311G++(d,p) basis set to analyse the electronic properties of the compounds

Introduction:

Schiff bases are highly valued for their simple synthesis, structural diversity, and wide range of applications from antiviral agents and agricultural uses to roles in photodetectors, photo stabilizers, and optical [1]. Their oxygen- and nitrogen-donor ligands exhibit significant biological properties and catalytic potential in both homogeneous and heterogeneous systems. The imine (–N=CH–) group facilitates transamination and racemization reactions [2], while key features such as chelation, thermal stability [3], and proton transfer mechanisms [4] enable further applications. Their high thermal stability makes them useful as stationary phases in gas chromatography [5]. Additionally, these compounds serve as catalysts in photoelectrochemical processes and as corrosion inhibitors for metals like mild steel, copper, aluminium, and zinc [6].

Benzoin, with its aromatic structure, is a key precursor that forms stable metal complexes with enhanced antioxidant, anticancer, and antimicrobial properties [7]. Meanwhile, 2 Aminopyridin is a valuable intermediate in pharmaceutical synthesis with promising anticancer, antimicrobial, and anti-inflammatory activities [8].

This study aims to prepare and characterize a Schiff base and its metal complexes (Co, Ni, Cu, Zn), prepare nano-complexes of Cu and Ni using the PLAL technique, evaluate their antioxidant activity (comparing nano vs. bulk forms), investigate their interaction with the VEGFR2 receptor (via Molecular Docking) as a potential cancer treatment, and analyse their electronic properties using DFT calculations.

Materials and Equipment Used

All chemicals and solvents used in the preparation were of high purity and obtained from Merck and Fluka companies. melting point apparatus (Stuarts SMP10) provided by the British company (STUART) was used, and the infrared spectra of the ligands and prepared complexes were recorded using an FTIR-8400S (Shimadzu) in the range of 400–4000 cm^{-1} with KBr pellets. UV-Vis spectra were measured using a Shimadzu UV-1650PC، in the range of 190–1000 nm The molar conductivity of the prepared complexes was measured using a 10^{-3} mol/L solution in ethanol at room temperature (25°C) with a digital conductivity meter CD-2005. Additionally, ^{1}H-NMR and ^{31}C-NMR spectra were recorded at the Central Laboratory - College of Education for Pure Sciences - University of Basra, Iraq, using a Bruker Spectrometer 400 MHz with DMSO-d6 as the solvent. Furthermore, an FSEM was employed in the University of Technology laboratories (Tescan MIRA III | Electron Microscopy) to perform Energy-Dispersive X-ray Spectroscopy (EDX) for elemental analysis, and an X-Ray Diffractometer (Philips PW 1730/10) was used for the necessary studies. Computational studies included Gaussian software [13] for density functional theory (DFT), AutoDock-4 for molecular docking, and Discovery Studio Visualizer for structural visualization.

Synthesis

Synthesis of Schiff Base [L1]

Using a 50 ml beaker, benzoin (2 g, 9.43 mmol) was dissolved in ethanol (10 ml), and a few drops of glacial acetic acid were added under continuous stirring for 15 minutes. Separately, 2-aminopyridine (0.90 g, 9.57 mmol) was dissolved in hot absolute ethanol (10 mL) in a (50 mL) round-bottom flask immersed in a hot water bath, forming a clear solution. The 2-aminopyridine solution was then gradually added to the first solution, resulting in a yellow-colored mixture. The reaction mixture was subjected to reflux at 80–85°C for 5 hours. After cooling, a pale-yellow precipitate formed. The precipitate was filtered, washed with cold ethanol, and yielded yellow needle-like crystals (2.1 g, 72% yield) with a melting point of 114°C, as illustrated in Scheme (1)

Synthesis of metal complexes

Synthesis of the Complex $[Co(L1)_2]\cdot H_2O$

In a 100 mL round-bottom flask, (0.24 g 0.085 mmole) of the ligand [L1] was placed in 10 mL of absolute ethanol with slight heating to ensure complete dissolution. Then, (0.1 g 0.42 mmole) of $CoCl_2\cdot 6H_2O$, dissolved in 10 mL of ethanol, was gradually added with continuous stirring. Upon addition, the colour changed from blue to pink, corresponding to a (M:L ratio of 1:2). The mixture was then refluxed for 4 hours at (80°C), resulting in the formation of a pink precipitate. The solution was left to allow the solvent to evaporate at room temperature, and after 3 days, pink needle-like crystals were obtained. The precipitate was washed with diethyl ether, and the solvent was Evaporate under vacuum. The yield of the precipitate was (71%) with a melting point of (290°C), as shown in Scheme (2).

Similarly, the complexes $[Ni(L1)_2]\cdot H_2O$, $[Cu(L1)_2]\cdot H_2O$, and $[Zn(L1)_2]\cdot H_2O$ were prepared using the same procedure. **Table (1)** shows the weight of the ligand used with each metal salt in the preparation of the complexes, the proposed molecular formulas of the prepared complexes, the yield of the complexes, and some of their physical properties, noting that the weight of the metal salt was 0.1 g for each complex.

Table 1: Molecular formulas and some physical properties of the prepared complexes

No.	Metal salt	Weight of Ligand (g)	Empirical formula	Color	M.P° C	Yield %
1.	$CoCl_2.6H_2O$	0.24	$[Co(L1)_2].H_2O$	Pink	290	71
2.	$CuCl_2.2H_2O$	0.34	$[Cu(L1)_2].H_2O$	Blue	130	63
3.	$Ni\ Cl_2\ .6H_2O$	0.24	$[Ni(L1)_2].H_2O$	Cyan	125	84
4.	$ZnCl_2{\cdot}2H_2O$	0.21	$[Zn(L4)_2].H_2O$	Pale yellow	150	85

Results and discussion

The complexes were synthesized in a molar ratio of 1:2, [M:L], and their molar conductivity in Ethanol was found to be in the range of 2.20–3.20 $\Omega.mol^{-1}.cm^2$, thus showing that all-metal complexes are non- electrolytic in nature.

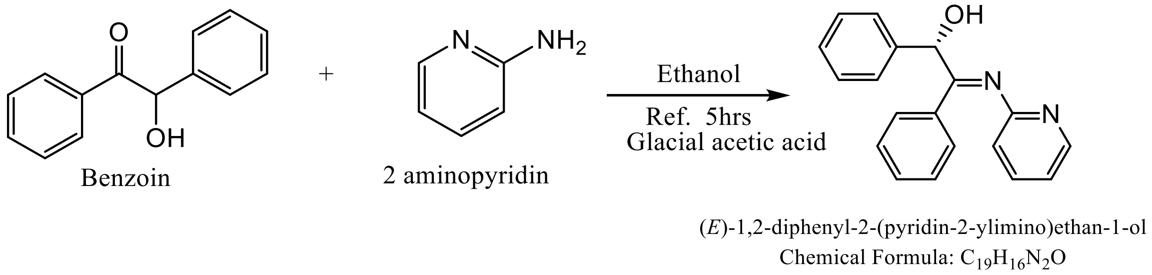

Scheme 1 Synthesis of Schiff Base [L1]

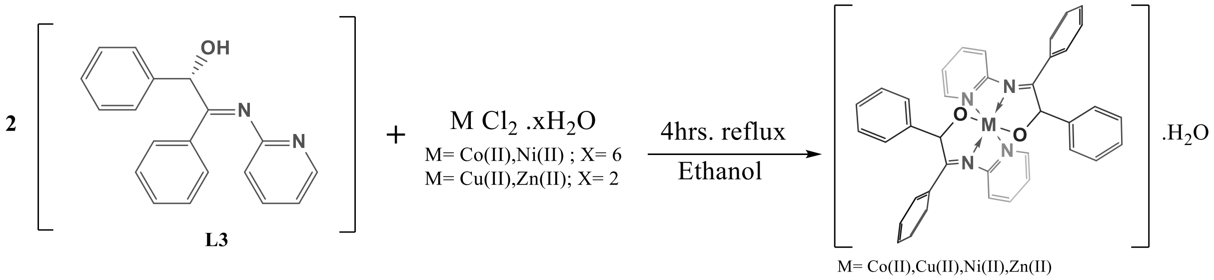

Scheme 2: Synthesis of Schiff Base [L1] Complex

Electronic spectra

UV-Visible Spectroscopic Analysis of Ligand [L1] and Its Complexes

The UV-visible spectrum of ligand [L1] exhibited two absorption peaks: the first at 201 nm (εmax = 586 $M^{-1}.cm^{-1}$), attributed to the (π→π*) transition, and the second at 340 nm (εmax = 19 $M^{-1}.cm^{-1}$), corresponding to the (n→π*) transition, reflecting the electronic structure of the ligand [9].

$[Co(L1)_2]\cdot H_2O$ complex, the spectrum showed a strong peak at 206 nm (48447 cm^{-1}, εmax = 1886 $M^{-1}.cm^{-1}$), indicating a charge transfer transition between cobalt and the ligand. No (d-d) transitions were observed due to their weak intensity, supporting an octahedral geometry[10].

$[Cu(L1)_2]\cdot H_2O$ complex revealed four peaks, the most intense at 199.2 nm (50201 cm^{-1}, εmax = 554 $M^{-1}.cm^{-1}$) for the (n→π*) transition, and another at 232.4 nm (43027 cm^{-1}, εmax = 388 $M^{-1}.cm^{-1}$) for the (π→π*) transition. Weak absorption bands in the visible region support an octahedral geometry[L11].

$[Ni(L1)_2]\cdot H_2O$ complex, four main peaks appeared, including one at 1017.6 nm (9827 cm^{-1}, εmax = 201 $M^{-1}.cm^{-1}$) for the ($3A_2g(F) \rightarrow 3T_2g(F)$) transition. Other peaks at 343.8 nm (n→π*), and 294.8 nm (metal-to-ligand charge transfer) confirm its octahedral coordination [12].

$[Zn(L1)_2]\cdot H_2O$ complex exhibited two peaks at 291.2 nm (34334 cm^{-1}, εmax = 136 $M^{-1}.cm^{-1}$) and 271 nm (36813 cm^{-1}, εmax = 128 $M^{-1}.cm^{-1}$), both attributed to (π→π*) transitions. Another peak at 871 nm (11483 cm^{-1}) corresponds to metal-to-ligand charge transfer (M→L), further supporting an octahedral structure[13].

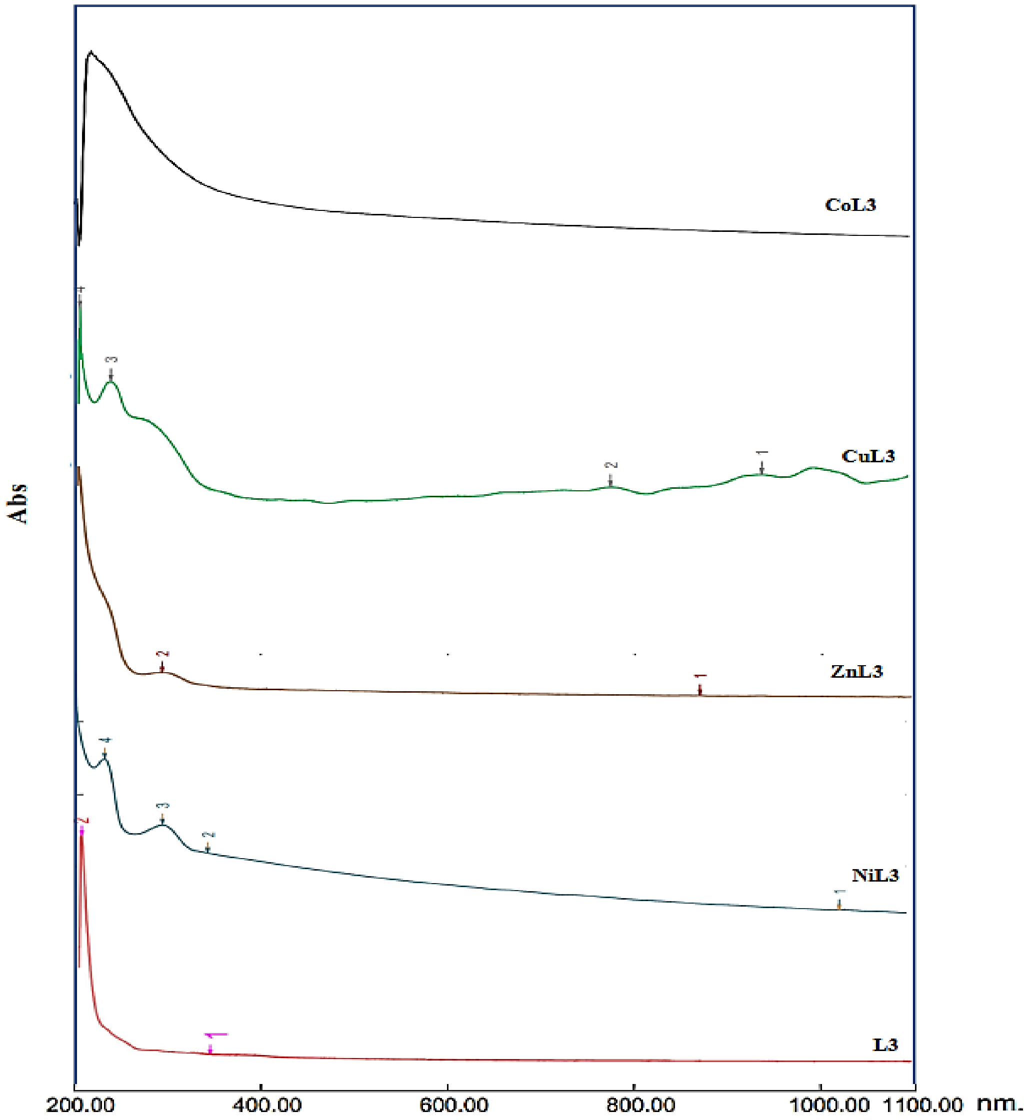

Fig (1) *UV-Visible Spectrum of the Ligand [L1] and Its Complexes*

IR spectra

FT-IR spectrum of the ligand [L1] and its metal complexes:

The FT-IR spectrum of the ligand [L1] (Schiff base) confirmed its successful formation through the appearance of the imine υ(C=N) band at 1629.85 cm^{-1}, along with the disappearance of the υ(NH_2) bands of 2-Aminopyridine (at 3178 cm^{-1}) and the ketonic υ(C=O) band of Benzoin (at 1677 cm^{-1}),. Aromatic υ(C=C) bands appeared at 1552 and 1589 cm^{-1}, and two bands for the (-OH) group were observed at 3223 and 1340 cm^{-1}.

For the metal complexes (Co(II), Cu(II), Ni(II), Zn(II)), changes indicative of metal coordination were noted, such as the shift of the υ(C=N) band to 1647.21–1631.78 cm^{-1} (compared to 1629.24 cm^{-1}). The spectra also revealed two new bands: the first, at 779.24–912.33 cm^{-1}, is attributed to υ(M–N) and the second, at 657.73–671.23 cm^{-1}, is attributed to υ(M–O) Other observations include the disappearance of the free (-OH) peak at 3223 cm^{-1} and the appearance of bands at 3228.84–3747.69 cm^{-1} corresponding to hydrate water molecules outside the coordination sphere. These changes confirm the formation of stable coordination complexes through the binding of the metal with the nitrogen atoms (imine and pyridine) and oxygen, with the presence of hydrate water in the structure [14-16], Figure 2, and the results are given in table 2.

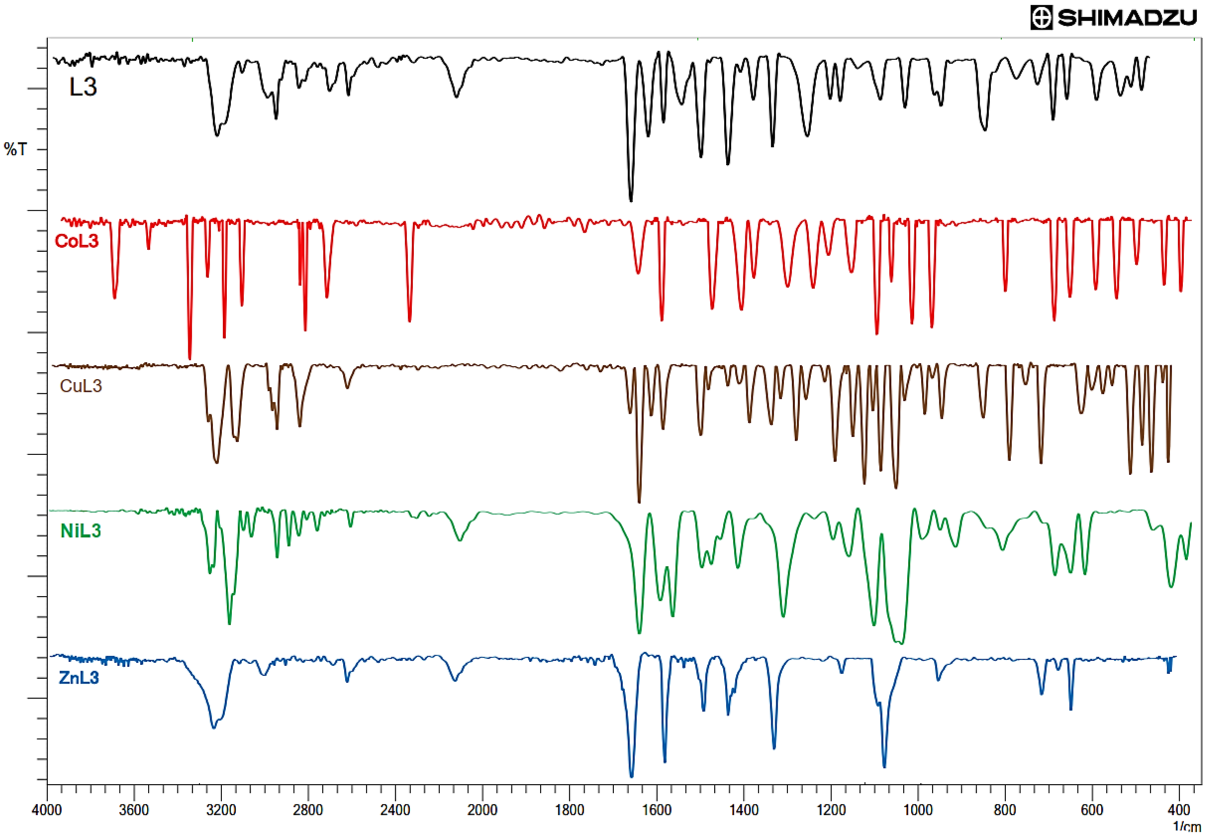

Fig. (2) *FT-IR spectrum of the Ligand [L1] and Its Complexes*

Table 2: Infrared spectra of the Schiff base [L1] and its metal complexes

compound	υ (C=N) imine (cm^{-1})	υ (C=N) in plane (cm^{-1})	υ (C-O) (cm^{-1})	δ (C-O) (cm^{-1})	(M-N) (cm^{-1})	(M-O) (cm^{-1})	Hydrate H_2O (cm^{-1})
(L1)	1589.34 (m, υ)	1629.85 (m, υ)	1157.29 (m, υ)	1294.24 (m, δ)	-	-	-
$[Co(L1)_2].H_2O$	1591.27 (s, υ)	1647.21 (s, υ)	1147.65 (s, υ)	1296.16 (s, δ)	786.96 (s)	671.23 (s)	3747.69 (s)
$[Cu(L1)_2].H_2O$	1581.63 (m, υ)	1631.78 (m, υ)	1145.72 (m, υ)	1296.16 (m, δ)	794.67 (m)	657.73 (m)	3229.70 (s)
$[Ni(L1)_2].H_2O$	1587.42 (m, υ)	1631.78 (m, υ)	1141.86 (m, υ)	1296.16 (m, δ)	786.96 (m)	665.44 (m)	3255.84 (m)
$[Zn(L1)_2].H_2O$	1552.70 (m, υ)	1631.78 (m, υ)	1136.07 (m, υ)	1296.16 (m, δ)	910.40 (m)	667.37 (m)	3228.84 (m)

NMR spectra

^{1}H NMR spectrum of ligand [L1] in DMSO-d_6 shows, at **δH = 9.52 ppm** is a singlet and corresponds to the hydroxyl (-OH) group, as the DMSO solvent shifts the signal downfield due to hydrogen bonding. The singlet at **δH = 8.36 ppm** belongs to the azomethine (-CH=N-) proton, which is evident from the integration values of the hydroxyl and azomethine groups. The signal at **δH = 6.97 ppm** arises from the methine proton (-CH-) adjacent to the hydroxyl group. The remaining peaks correspond to aromatic protons, as shown in **Figure 3**.

^{13}C NMR spectrum Revealed singlets: the most downfield-shifted signal at **δ 158.63 ppm** corresponds to the imine carbon (C=N, C3), while the signal at **δ 156.25 ppm** belongs to the phenolic ring carbon directly attached to the hydroxyl group (C-OH, C2). Pyridine ring carbons appear in the downfield region (**δ 143.72 ppm**), and other aromatic CH carbons are observed in the range **δ 133.17 – 122.90 ppm**. The shielded aromatic CH carbons (near the OH group) resonate upfield at **δ 115.40 ppm** and **δ 114.95 ppm**. [17] **(Figure (4)).**

^{1}H NMR spectrum of **$[Cu(L1)_2.H_2O]$ (Figure (5))**: A signal at (δH = 2.5 ppm) for the solvent; (δH = 7.49 ppm) for an aromatic proton; (δH = 7.25 ppm) for two benzene protons; (δH = 6.67 ppm) for two (N=C–H) protons; (δH = 4.03 ppm) for four (CH_2–O) protons; and a water signal at (δH = 3.34 ppm).

^{13}C NMR spectrum of **$[Cu(L1)_2.H_2O]$ (Figure (6))**: A signal at (δC = 39.52 ppm) for the solvent carbons; signals at (δC = 129.65–127.63 ppm) for the benzene carbons; signals at (δC = 99.54–99.31 ppm) for the (C=N) carbons or those close to copper; signals for the pyridine rings; and two signals at (δC = 71.22, 71.12 ppm) for the (CH_2–O) carbons [18].

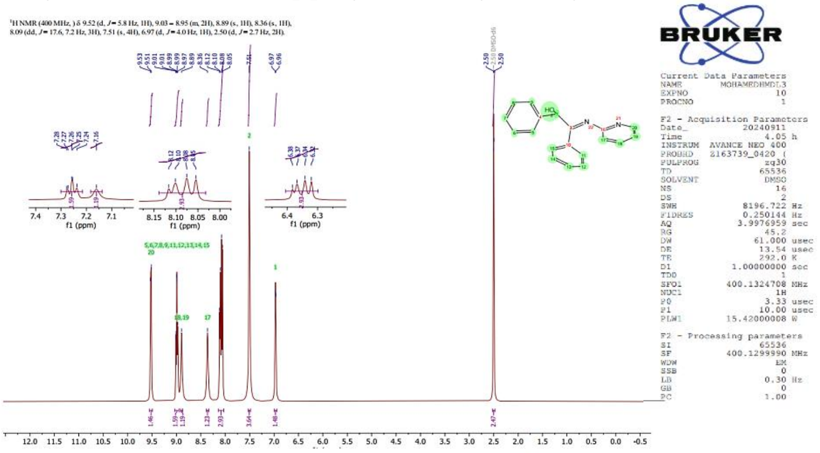

```
Current Data Parameters
NAME           MOHAMEDHMDL3
EXPNO                    10
PROCNO                    1

F2 - Acquisition Parameters
Date_              20240911
Time                 4.05 h
INSTRUM     AVANCE NEO 400
PROBHD     Z163739_0420 (
PULPROG                zg30
TD                    65536
SOLVENT                DMSO
NS                       16
DS                        2
SWH                8196.722 Hz
FIDRES             0.250144 Hz
AQ                3.9976959 sec
RG                     45.2
DW                   61.000 usec
DE                    13.54 usec
TE                    292.0 K
D1               1.00000000 sec
TD0                       1
SFO1            400.1324708 MHz
NUC1                     1H
P0                     3.33 usec
P1                    10.00 usec
PLW1            15.42000008 W

F2 - Processing parameters
SI                    65536
SF              400.1299990 MHz
WDW                      EM
SSB                       0
LB                     0.30 Hz
GB                        0
PC                     1.00
```

Fig. 3 *^{1}H-NMR Spectrum of ligand [L1]*

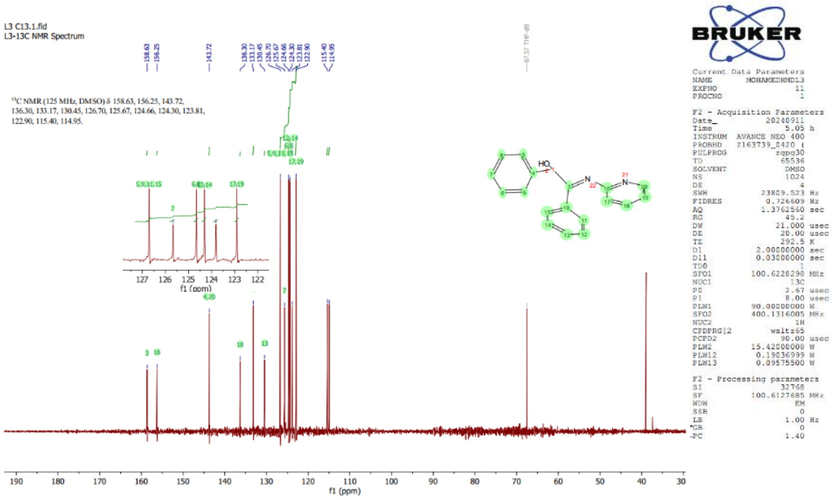

Fig. 4 *^{13}C-NMR Spectrum of ligand [L1]*

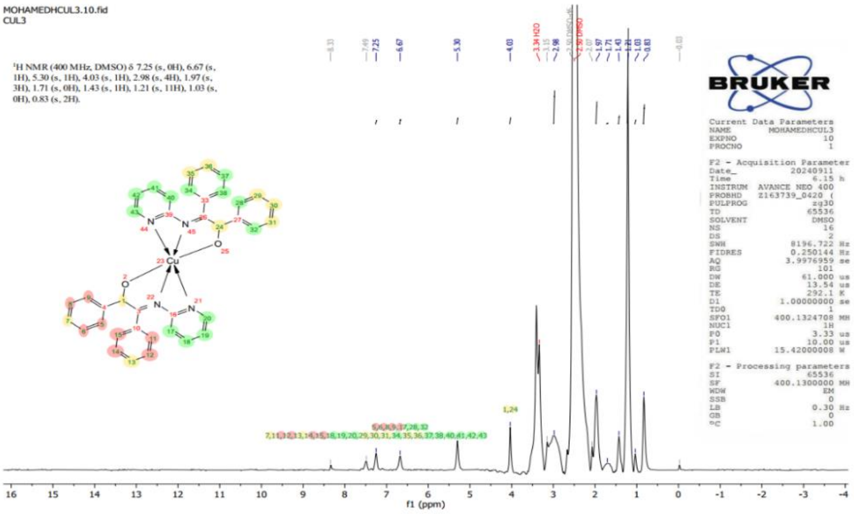

Fig. 6 *^{1}H-NMR Spectrum of [Cu(L1)$_2$.H$_2$O]*

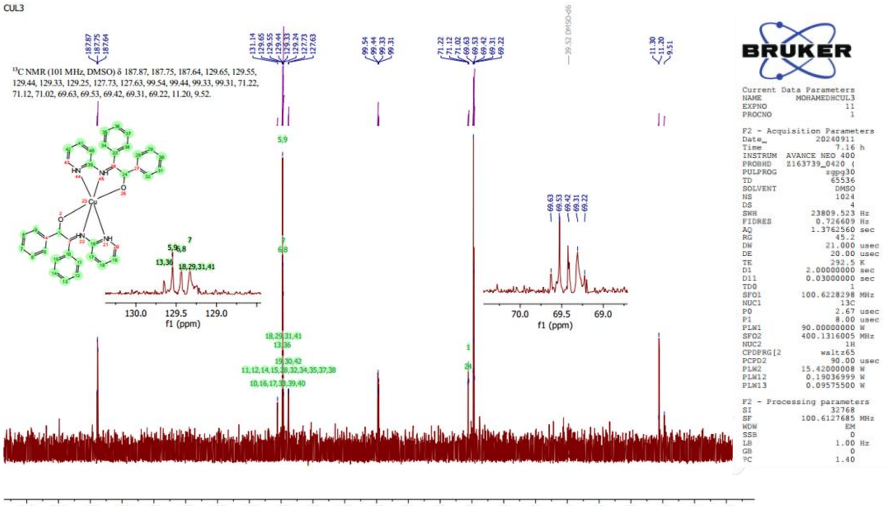

Fig. 5 *^{13}C-NMR Spectrum of [Cu(L1)$_2$.H$_2$O]*

Preparation of nano-complexes

The nanocomplexes **[Cu(L1)$_2$·H$_2$O]** and **[Ni(L1)$_2$·H$_2$O]** were synthesized using the Pulsed Laser Ablation in Liquid (PLAL) technique, where short laser pulses vaporize the solid material submerged in a liquid, forming a transient plasma that leads to the formation of stable nanoparticles (226). The particles were characterized using SEM to determine morphology and surface distribution, XRD for crystal structure analysis, and EDX for elemental analysis [19].

Characterization of Nano-Complexes

Field Emission Scanning Electron Microscopy (FESEM) Analysis

The nanoparticles of the complex **$[Cu(L1)_2]\cdot H_2O$** exhibited a diameter of **D_1 = 136 nm**, as shown in **Figure (7)** under varying magnification powers. Particles with rounded edges were observed, indicating potential **high crystallinity or surface interactions** [20].
For the complex **$[Ni(L1)_2\cdot H_2O]$**, the nanoparticle diameter was measured as **D_1 = 58.25 nm**, as illustrated in **Figure (8)**. Crystalline spherical shapes with some sharp edges were noted, attributed to **high crystallinity**.

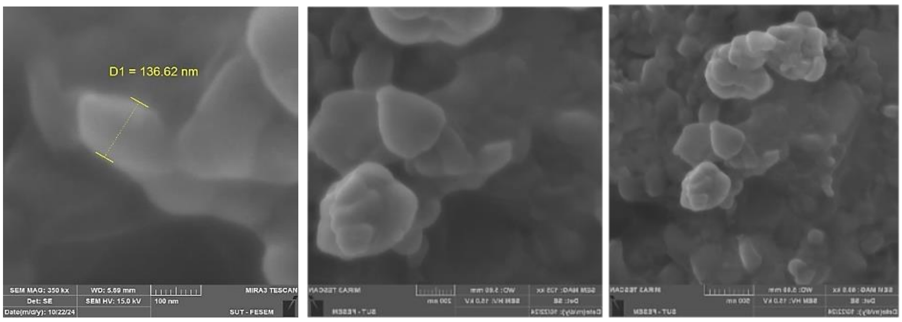

Fig. *7 (FESEM) at different magnification powers of the $[Cu(L1)_2]H_2O$ nanocomplex*

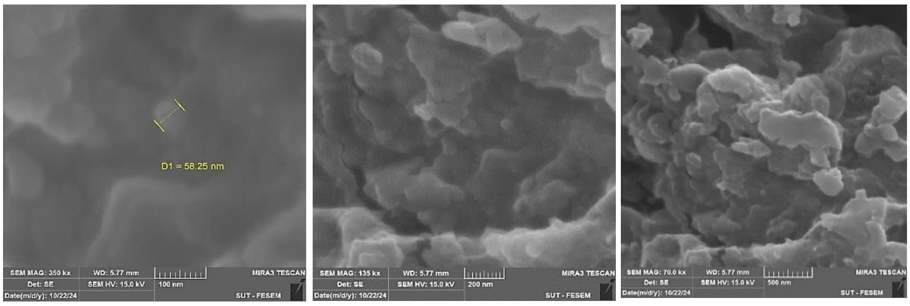

Fig. 8 (*FESEM) at different magnification powers of the $[Ni(L1)_2]H_2O$ nanocomplex*

X-ray Diffraction (XRD) Analysis

(XRD) Spectrum of the Complex $[Cu(L1)_2]\cdot H_2O$ and $[Ni(L1)_2]\cdot H_2O$

The XRD pattern of the complex **$[Cu(L1)_2\cdot H_2O]$** (**Figure 9**) showed a 2θ range between (10.849° and 73.62°), with (d-spacing) values ranging from (0.8148 to 0.1286 nm). The main peak appeared at (2θ = 11.699°) with (100% intensity), along with other peaks at (2θ = 21.700°, 19.161°, and 29.341°). The pattern indicates the presence of a major crystalline phase with possible secondary phases or variations in crystal orientations. The variation in peak width suggests differences in crystal sizes and lattice distortions, and the broad peak at (2θ = 42.68°) indicates a nanocrystalline size [21].

The XRD spectrum of the **$]Ni(L1)_2\cdot H_2O]$** complex ranges from (2θ = 10.849° to 73.62°) (**Figure 10**), with d-spacing values between 0.8148 and 0.1286 nm. The main peak at (2θ = 11.699°) with 100% intensity indicates the primary crystalline phase, while lower-intensity peaks suggest secondary phases or variations in crystal orientations. Peak widths range from 0.18° to 2.3° at (2θ = 61.7°), reflecting differences in crystal sizes or lattice distortions. The broad peak at (2θ = 42.68°) indicates a nanocrystalline structure [22].

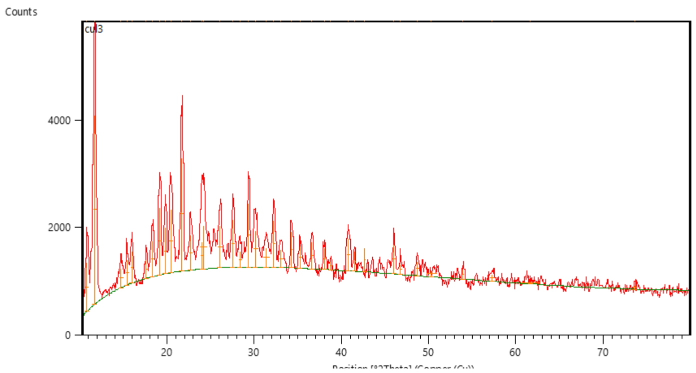

Fig. 9: *(XRD) Spectrum of the* $[Cu(L1)_2]\cdot H_2O$

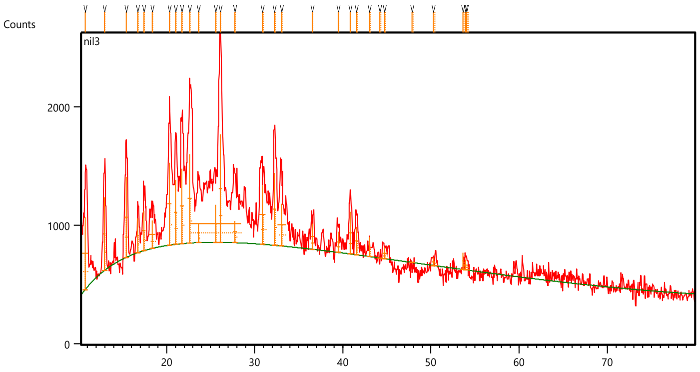

Fig.10: *(XRD) Spectrum of the* $[Ni(L1)_2]\cdot H_2O$

Characterization of the Nanocomplexes by (EDX)

The spectrum of the complex $\mathbf{[Cu(L1)_2\cdot H_2O]}$ shows distinct peaks, including copper peaks at (9.0 keV) for the Lα line and (8 keV) for the Kα line, as well as a clear oxygen peak at (0.5–0.6 keV) originating from the ligand bound to **copper**. Additionally, there are peaks for gold (**Au**) resulting from the sample holder, a carbon (**C**) peak at (0.27 keV), and a small nitrogen (N) peak at (0.3 keV) due to the low energy of its spectral lines. Meanwhile, the complex $\mathbf{[Ni(L1)_2\cdot H_2O]}$ exhibits **nickel** peaks at (7.5 keV) and (8.3 keV) for the Kα and Kβ lines, respectively, along with a low-intensity oxygen peak at (0.5–0.6 keV), gold (**Au**) peaks originating from the sample holder or metallic coating, a high-intensity carbon (**C**) peak at (0.27 keV), and a low-intensity nitrogen (**N**) peak at (0.3 keV)[23] as shown in Figures **(11 - 12).** (L1)

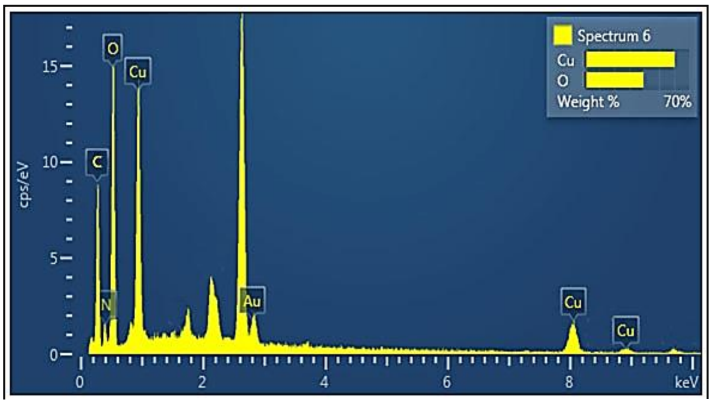

Fig. ***(11):*** *EDX spectrum of the complex* $[Cu(L1)_2]\cdot H_2O$

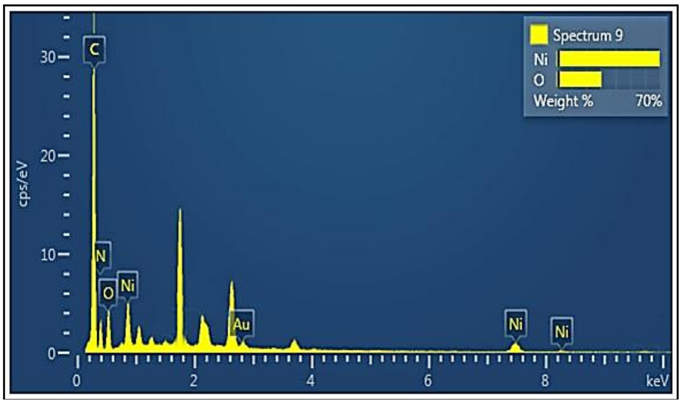

Fig. (12): *EDX spectrum of the complex* $[Ni(L1_2]\cdot H_2O$

Study of density functional theory (DFT) and orbital energies

Gaussian 09 was used to obtain an optimized geometry and calculate the energy gap (ΔE) between the HOMO and LUMO orbitals using Density Functional Theory (DFT) and the hybrid functional B3LYP with the basis set (6-31G), as shown in **Table (3)**. The highest occupied molecular orbital (HOMO) and the lowest unoccupied molecular orbital (LUMO) are referred to as "Frontier orbitals" because they are largely responsible for the chemical and spectral properties of the molecule, determining its reactivity and stability; a higher LUMO energy indicates greater stability, whereas a lower LUMO energy suggests a higher tendency to accept electrons, and conversely, a higher HOMO energy indicates a greater tendency to lose electrons and undergo transitions from the ground state to the excited state [24]. The data in the table show that the energy gap (ΔE), such as that for [CoL1] ((0.25 eV)) and [ZnL1] ((0.31

eV)), implies high chemical reactivity, while a large gap, for CuL1 ((1.95 eV)), indicates low chemical reactivity and high stability; meanwhile, [L1] ((0.55 eV)) and [NiL1] ((0.87 eV)) fall in the middle in terms of reactivity and stability[25],as shown in Figures (13).

Table 3: HOMO-LUMO orbital energy results for the ligand [L1] and its complexes.

#	Comp	E HOMO eV	E LUMO eV	$\vert \Delta E \vert$ eV
1.	L1	-7.56	-7.011	0.55
2.	CoL1	-3.75	-3.503	0.25
3.	CuL1	-4.44	-2.487	1.95
4.	NiL1	-3.43	-2.558	0.87
5.	ZnL1	-7.16	-6.850	0.31

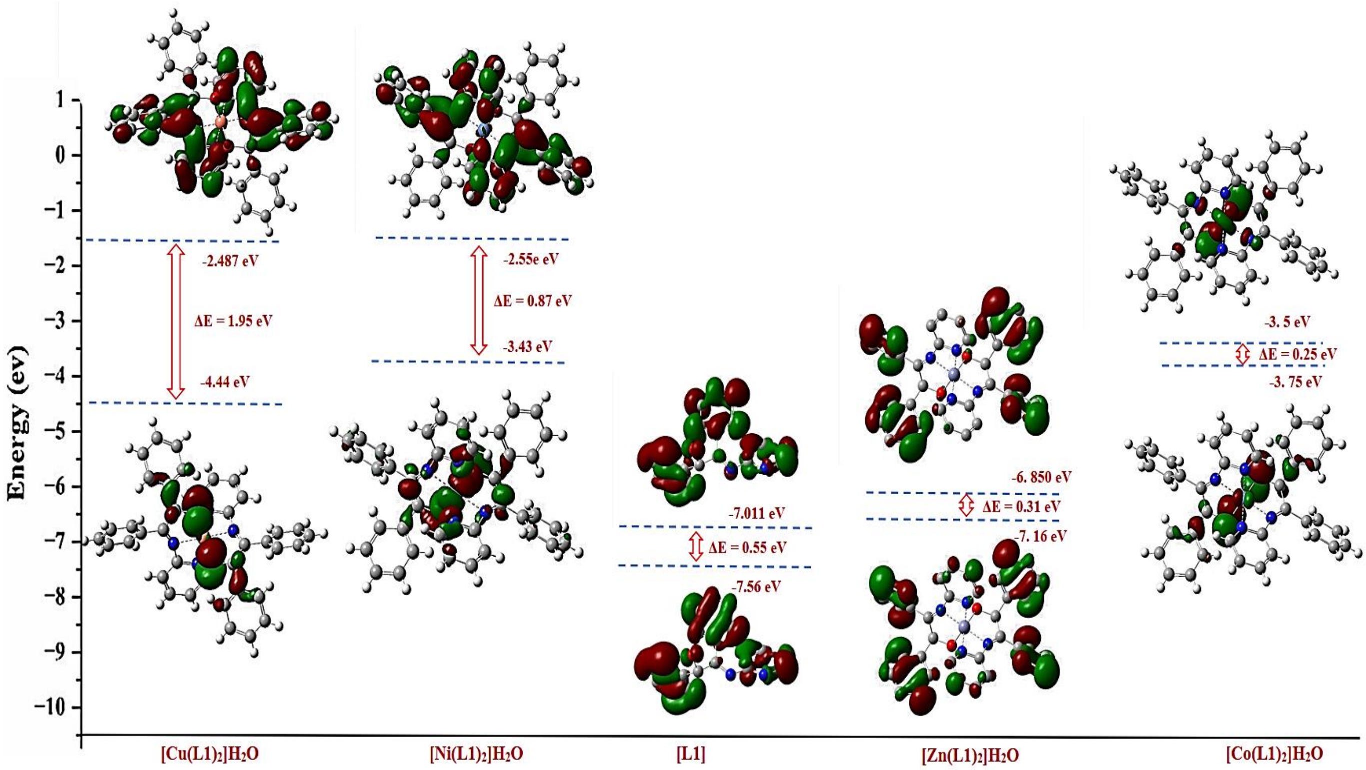

Fig. 13 *Frontier molecular orbitals (FMO) analysis of the ligand [L1] and its complexes*

Molecular Docking Results

The molecular docking energy of the ligand [L1] and its zinc complex $[Zn(L1)_2]\cdot H_2O$ (Zinc is of relatively low toxicity to humans) was studied and compared with the binding energy of the reference drug Sunitinib (Figure 3-97), a multi-kinase inhibitor targeting VEGFR, PDGFR, and c-Kit, used in treating certain tumours such as renal cell carcinoma and gastrointestinal stromal tumours (GIST). Sunitinib contains an indolinone core with functional groups similar to those in the ligand, enhancing its affinity for the target protein (VEGFR2), a tyrosine kinase receptor that plays a key role in angiogenesis. Molecular docking analysis showed that the binding energy of [L1] was (-7 Kcal/mol), which is higher than that of Sunitinib (-6.5 Kcal/mol), indicating stronger interactions. This is attributed to π–Anion interactions with negatively charged aspartate, π–Alkyl/π–Sigma interactions with hydrophobic chains, and potential hydrogen bonding or van der Waals interactions. The zinc complex $[Zn(L1)_2]\cdot H_2O$ exhibited even higher binding energies than the free ligand and the reference drug due to the coordination of amino acids with the zinc atom, making it a promising candidate for new drug development [26], as shown in Table (4) and Figures (14-16).

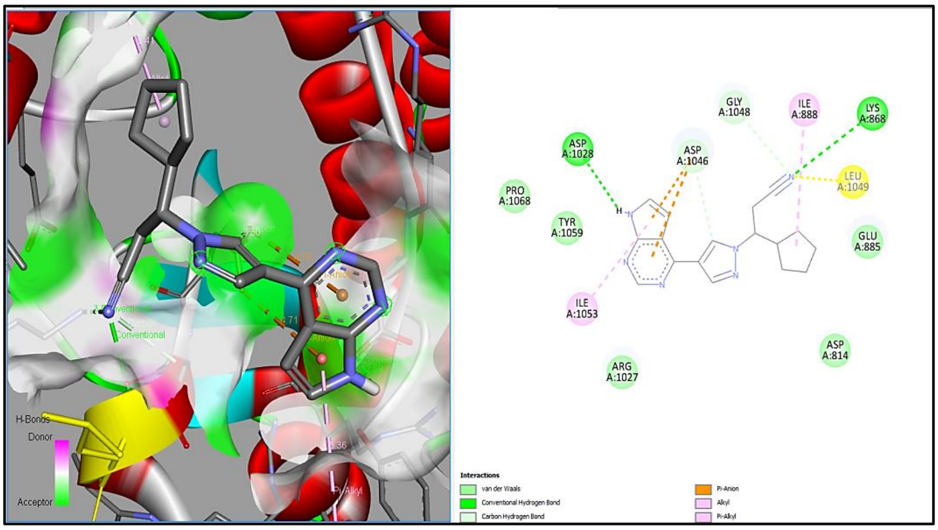

Fig. (14) *Molecular docking of the (VEGFR2) protein with the drug (Sunitinib)*.

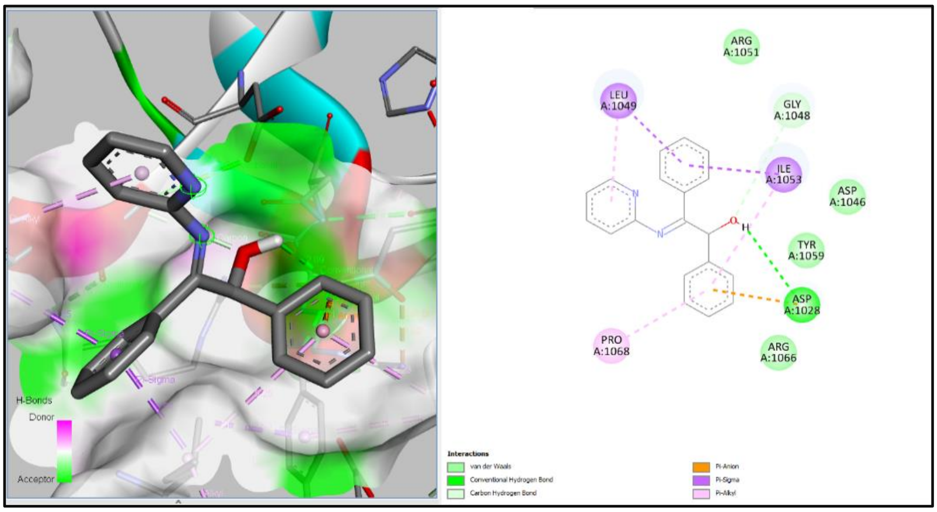

Fig. (15) *Molecular docking of the (VEGFR2) protein with the ligand (L1).*

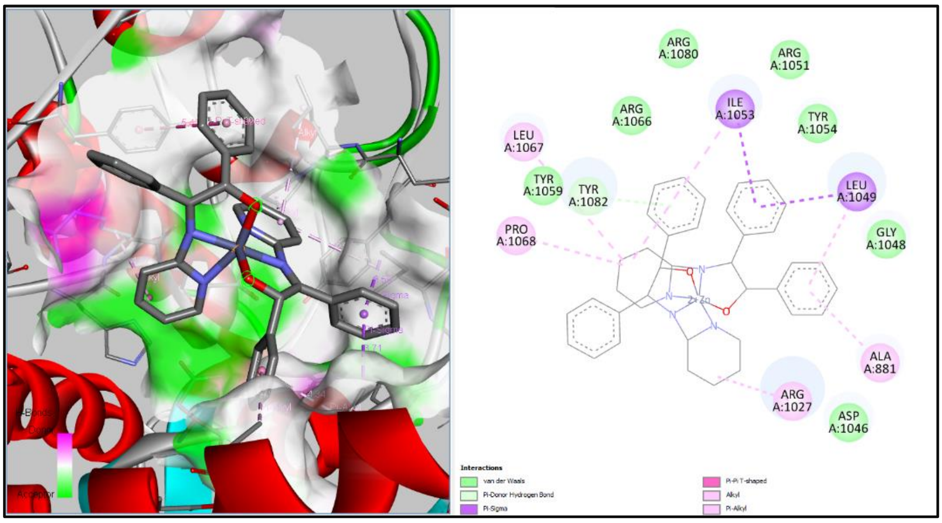

Fig. (16) *Molecular docking of the (VEGFR2) protein with $[Zn(L1)_2]\cdot H_2O$*.

Evaluation of the Antioxidant Activity of the Prepared Nanocomplexes at the Concentration Corresponding to Half-Maximal Inhibitory Concentration (IC_{50}) and Comparison with Their Bulk-Sized Complexes.

The **[NiL1-Nano]** complex exhibited a lower **IC_{50} value (<48 µg/mL)** compared to the **[CuL1-Nano]** complex (IC50 = 62 µg/mL), indicating that **[NiL1-Nano]** is more effective in inhibiting oxidation processes. Both nano-complexes significantly outperformed their non-nano counterparts, with an improvement rate exceeding **40%** for both complexes [27]. as shown in Figures (17).

Table 4: Molecular docking values for the ligand (L1) and the zinc complex compared to the drug (Sunitinib), along with bond types and interactions

Compound	Affinity (kcal/mol)	Types of Bonds/Interactions
Sunitinib	-6.5	- Conventional Hydrogen Bonds with residues: ASP A.1029, ASP A.1046. - Carbon Hydrogen Bonds with residues: ILE A.888, PRO A.1068. - van der Waals Interactions with residues: ILE A.1053, TYR A.1059.
L1	-7	- Hydrogen Bonds with residues: ASP A:1046, ARG A:1051. - van der Waals Interactions with residues: LEU A:1049, GLY A:1048. - Carbon Hydrogen Bonds with residues: TYR A:1059.
$(Zn(L1)_2.H_2O$	-8.8	- Hydrogen Bonds with residues: ARG A:1080, ARG A:1051. - Zinc Coordination Interactions. - van der Waals Interactions with residues: TYR A:1067, LEU A:1049.

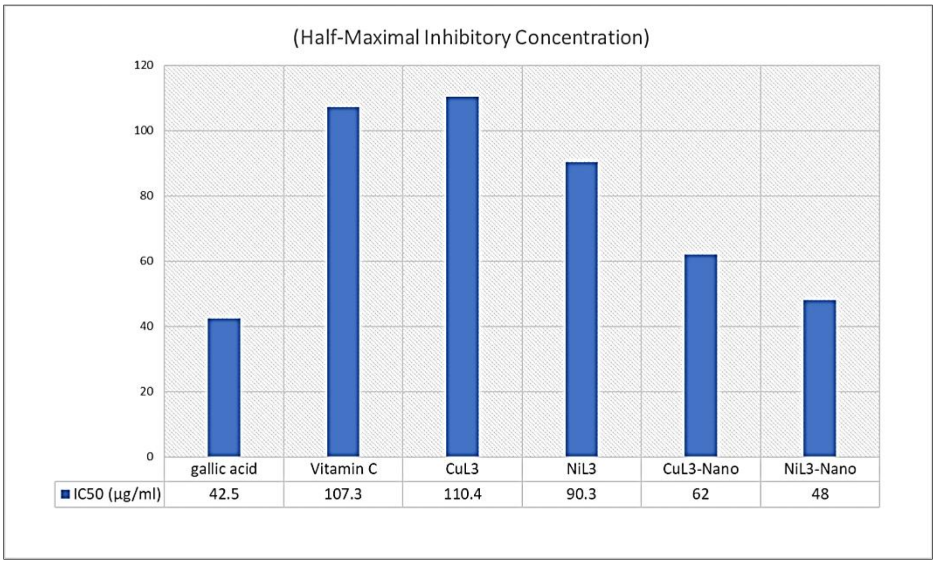

Fig. (17): *Comparison of IC_{50} Values for the Nanocomplexes (NiL1-Nano) and (CuL1-Nano) with Their Corresponding Bulk Complexes, the Standard Antioxidant (Gallic Acid), and Vitamin C.*

Conclusions

In this study, a new Schiff base [L1] was synthesized from benzoin and 2-Aminopyridine, along with its Co(II), Ni(II), Cu(II), and Zn(II) complexes in a 1:2 ligand-to-metal ratio. ^{1}H NMR, ^{13}C NMR, FT-IR, UV-Vis, and molar conductivity measurements confirmed that the prepared complexes adopt an octahedral geometry. The Cu(II) and Ni(II) nanocomplexes were also fabricated via Pulsed Laser Ablation in Liquid (PLAL), and FESEM, EDX, and XRD analyses revealed the formation of uniform nanoparticles with well-defined crystalline structures. These compounds exhibited significant antioxidant activity, with IC_{50} values comparable to standard antioxidants and their bulk counterparts, and the nanocomplexes showed notably enhanced efficacy. Molecular docking studies demonstrated strong binding interactions with the 2VEGFR receptor, supporting the potential use of these compounds as anti-angiogenic agents in liver and kidney cancer therapies. Furthermore, DFT calculations at the B3LYP/6-311G++(d,p) level provided detailed charge and orbital distribution profiles that explain their chemical and biological activities.

References

1. Hasibul Islam, M., & Abdul Hannan, M. (2024). Schiff bases: Contemporary synthesis, properties, and applications. In *Novelties in Schiff Bases*. IntechOpen.
2. Patai, S. (1970). *The chemistry of the carbon-nitrogen double bond*. Wiley-Interscience.
3. Catalano, A., Sinicropi, M. S., Iacopetta, D., Ceramella, J., Mariconda, A., Rosano, C., & et al. (2021). A review on the advancements in the field of metal complexes with Schiff bases as antiproliferative agents. *Applied Sciences*, 11(13), 6027. https://doi.org/10.3390/app11136027
4. Du, Z., Zhang, F., Lin, H., Guo, W., Tian, M., Yu, K., & Qu, F. (2023). Thermal-response proton conduction in Schiff base-incorporated metal-organic framework hybrid membranes under low humidity based on the excited-state intramolecular proton transfer mechanism. *ACS Applied Materials & Interfaces*, 15(7), 10064–10074. https://doi.org/10.1021/acsami.2c23170
5. Zhao, Y., Zhang, T., Xiong, H., & Wang, F. (2021). Bridge for the thermodynamics and kinetics of electrochemical corrosion: Modelling on dissolution, ionization, diffusion, and deposition in metal/solution interface. *Corrosion Science*, 191, 109763. https://doi.org/10.1016/j.corsci.2021.109763
6. Music, D., Geyer, R. W., & Schneider, J. M. (2016). Recent progress and new directions in density functional theory-based design of hard coatings. *Surface and Coatings Technology*, 286, 178–190. https://doi.org/10.1016/j.surfcoat.2015.12.021
7. Ismail, H. A., & Abed, R. R. (2023). Synthesis, characterization, and biological activity assessment of new metal complexes of Schiff bases produced from benzoin. *Al-Kitab Journal of Pure Science*, 7(1), 27–41. https://doi.org/10.32441/kjps.07.01.p3ISNRA
8. Rao RN, Chanda K. 2-Aminopyridine - an unsung hero in drug discovery. Chem Commun (Camb) [Internet]. 2022 [cited 2025 Mar 20];58(3):343–82. Available from: https://pubs.rsc.org/en/content/articlelanding/2021/xx/d1cc04602k/unauth
9. Iggo, J. A., & Luzyanin, K. (2020). *NMR spectroscopy in inorganic chemistry* (2nd ed.). Oxford University Press.
10. Sotiles, A. R., Massarotti, F., Pires, J. C. de O., Facchin Ciceri, M. E., & Budziak Parabocz, C. R. (2019). Cobalt complexes: Introduction and spectra analysis. *Orbital: Electron Journal of Chemistry*, 11(6). https://doi.org/10.17807/orbital.v11i6.1242
11. Masternak, J., Zienkiewicz-Machnik, M., Łakomska, I., Hodorowicz, M., Kazimierczuk, K., Nosek, M., & et al. (2021). Synthesis and structure of novel copper(II) complexes with N,O- or N,N-donors as radical scavengers and a functional model of the active sites in metalloenzymes. *International Journal of Molecular Sciences*, 22(14), 7286. https://doi.org/10.3390/ijms22147286
12. Li, Y.-J., Guo, S.-Z., Feng, T., Xie, K.-F., & Dong, W.-K. (2021). An investigation into three-dimensional octahedral multi-nuclear Ni(II)-based complexes supported by a more

flexible salamo-type ligand. *Journal of Molecular Structure*, 1228, 129796. https://doi.org/10.1016/j.molstruc.2020.129796

13. Dege, N., Tamer, Ö., Şimşek, M., Avcı, D., Yaman, M., Başoğlu, A., & et al. (2022). Experimental and theoretical approaches on structural, spectroscopic (FT-IR and UV-Vis), nonlinear optical, and molecular docking analyses for Zn(II) and Cu(II) complexes of 6-chloropyridine-2-carboxylic acid. *Applied Organometallic Chemistry*, 36(6). https://doi.org/10.1002/aoc.6678
14. Kareem, M. J., Al-Hamdani, A. A. S., Jirjees, V. Y., Khan, M. E., Allaf, A. W., & Al Zoubi, W. (2021). Preparation, spectroscopic study of Schiff base derived from dopamine and metal Ni(II), Pd(II), and Pt(IV) complexes, and activity determination as antioxidants. *Journal of Physical Organic Chemistry*, 34(3). https://doi.org/10.1002/poc.4156
15. Yousif, E., Majeed, A., Al-Sammarrae, K., Salih, N., Salimon, J., & Abdullah, B. (2017). Metal complexes of Schiff base: Preparation, characterization and antibacterial activity. *Arabian Journal of Chemistry*, 10, S1639–S1644. https://doi.org/10.1016/j.arabjc.2013.06.006 Internet Archive Scholar
16. Chalmers, J. M., & Griffiths, P. R. (Eds.). (2002). *Handbook of vibrational spectroscopy*. Wiley.
17. Silverstein, R. M., Webster, F. X., Kiemle, D. J., & Bryce, D. L. (2014). *Spectrometric identification of organic compounds* (8th ed.). John Wiley & Sons.
18. Shin, J., Lim, M. H., & Han, J. (2024). NMR spectroscopic investigations of transition metal complexes in organometallic and bioinorganic chemistry. *Bulletin of the Korean Chemical Society*, 45(7), 593–613. https://doi.org/10.1002/bkcs.12853
19. Verma, A. K., & Soni, R. K. (2023). Laser ablation synthesis of bimetallic gold-palladium core@shell nanoparticles for trace detection of explosives. *Optics & Laser Technology*, 163, 109429. https://doi.org/10.1016/j.optlastec.2023.109429
20. Zhang, X., Li, Y., Sun, X., Kishen, A., Deng, X., Yang, X., et al. (2014). Biomimetic remineralization of demineralized enamel with nano-complexes of phosphorylated chitosan and amorphous calcium phosphate. *Journal of Materials Science: Materials in Medicine*, 25(12), 2619–2628. https://doi.org/10.1007/s10856-014-5285-2
21. Ali, A., Chiang, Y. W., & Santos, R. M. (2022). X-ray diffraction techniques for mineral characterization: A review for engineers of the fundamentals, applications, and research directions. *Minerals*, 12(2), 205. https://doi.org/10.3390/min12020205
22. Bin Mobarak, M., Hossain, M. S., Chowdhury, F., & Ahmed, S. (2022). Synthesis and characterization of CuO nanoparticles utilizing waste fish scale and exploitation of XRD peak profile analysis for approximating the structural parameters. *Arabian Journal of Chemistry*, 15(10), 104117. https://doi.org/10.1016/j.arabjc.2022.104117
23. Anand, G. T., Nithiyavathi, R., Ramesh, R., John Sundaram, S., & Kaviyarasu, K. (2020). Structural and optical properties of nickel oxide nanoparticles: Investigation of antimicrobial applications. *Surfaces and Interfaces*, 18, 100460. https://doi.org/10.1016/j.surfin.2020.100460
24. Construction frontier molecular orbital prediction model with transfer learning for organic materials — Xinyu Peng et al., npj Computational Materials, 2024. DOI: 10.1038/s41524-024-01403-6
25. Isravel, A. D., Jeyaraj, J. K., Thangasamy, S., & John, W. J. (2021). DFT, NBO, HOMO-LUMO, NCI, stability, Fukui function and hole–electron analyses of tolcapone. *Computational and Theoretical Chemistry*, 1202, 113296. https://doi.org/10.1016/j.comptc.2021.113296
26. Tavares, F. M., Gomes, A. C., Assunção, E. M., de Medeiros, J. L. S., Scotti, M. T., Scotti, L., et al. (2022). Virtual screening, and molecular docking: Discovering novel c-KIT inhibitors. *Current Medicinal Chemistry*, 29(2), 166–188. https://doi.org/10.2174/0929867328666210915102920

27. Sargazi, S., Laraib, U., Er, S., Rahdar, A., Hassanisaadi, M., Zafar, M. N., et al. (2022). Application of green gold nanoparticles in cancer therapy and diagnosis. *Nanomaterials*, 12(7), 1102. https://doi.org/10.3390/nano12071102

IRAQI Academic Scientific Journals

Samarra Journal of Pure and Applied Science

SJPAS
مجلة سامراء للعلوم الصرفة والتطبيقية

www.sjpas.com

p ISSN: 2663-7405
e ISSN: 2789-6838

تحضير وتشخيص ودراسة مضادات الأكسدة والحسابات النظرية والالتحام الجزيئي لقاعدة شف وبعض معقداتها الفلزية النانوية (II)

محمد حسن عبد[1]، لقاء عبد الكريم[2]، مها صالح حسين[3]
1 قسم الكيمياء التطبيقية، كلية العلوم التطبيقية، جامعة سامراء، العراق
2 قسم الكيمياء، كلية التربية للعلوم الصرفة، جامعة بغداد، العراق
3 قسم الكيمياء، كلية التربية للعلوم الصرفة، جامعة سامراء، العراق

البحث مستل من أطروحة دكتوراه الباحث الاول

معلومات البحث:

تأريخ الاستلام: 2025/04/08
تاريخ التعديل: 2025/05/08
تأريخ القبـــول: 2025/05/15
تاريخ الـنشر: 2026/04/10

الكلمات المفتاحية:

دالة الكثافة الوظيفية، معقدات نانوية، الالتحام الجزيئي، قواعد شف، المدارات الحدودية.

معلومات المؤلف

الايميل:
الموبايل:

الخلاصة:

تم تحضير قاعدة شف (((E)-1,2-diphenyl-2-(pyridin-2-ylimino) ethan-1-ol) من (Benzoin) و(2Aminopyridine) ومعقداتها مع أيونات Co (II)، Ni (II)، Cu (II)، و Zn (II). بنسبة (1:2) (ليكاند: الملح) تم تشخيص المركبات المحضرة و^{1}H-NMR، و^{13}C-NMR، وتحليل FT-IR، UV-Vis وقياسات التوصلية المولارية. كما تم تحضير المعقدات النانوية لـ Cu (II) و Ni (II) باستخدام تقنية الليزر النبضي في سائل (PLAL)، وشخصت بواسطة المجهر الإلكتروني الماسح (FESEM)، وتحليل الطاقة المشتتة للأشعة السينية (EDX)، وتحليل حيود الأشعة السينية (XRD). قُيِّمت نشاطاتها المضادة للأكسدة باستخدام قيم IC$_{50}$ ، ومُقارنتها بمضادات الأكسدة القياسية ونظائرها ذات الحجم الطبيعي. كما استُخدمت دراسات الالتحام الجزيئي لاستكشاف تفاعلات الربط مع مستقبل 2-VEGFR2 وهو هدف رئيسي في علاجات سرطان الكبد والكلى نظرًا لدوره في تكوّن الأوعية الدموية. علاوةً على ذلك، أُجريت حسابات نظرية دالة الكثافة (DFT) عند مستوى B3LYP باستخدام مجموعة الأساس 311-6 G++(d,p) لتحليل الخواص الإلكترونية للمركبات.